

Original Article

Finite element analysis of asymmetrical retinal hemorrhages in shaken baby syndrome

Elliot H. Choi 1t, Jose A. Colmenarez 2t, John D. Hong 1, Kourosh Shahraki 1, Linxia Gu 2, Donny W. Suh 1

- ¹ Gavin Herbert Eye Institute, Department of Ophthalmology, University of California, Irvine, CA, USA
- ² Department of Biomedical Engineering and Science, Florida Institute of Technology, Melbourne, FL, USA
- † These authors contributed equally.

ABSTRACT

Background: Despite the common association between bilateral retinal hemorrhage and shaken baby syndrome (SBS), unilateral retinal hemorrhage does not necessarily exclude this diagnosis. This study used computational simulations to elucidate the biomechanical phenomena within the eye under asymmetrical shaking forces.

Methods: Finite element analysis (FEA) incorporating the vitreous, vitreoretinal interface, retinal layers, and retinal vessels was performed under asymmetrical shaking conditions. To assess the stress-strain response at the preretinal, intraretinal, and subretinal locations, we divided the retinal mesh into three equally spaced layers with an element height of 0.083 mm. The remaining space within the retina was filled with the vitreous humor and attached to it via the main retinal vessels extracted from a standard fundus image. The resulting changes in shear stress and intraocular pressure (IOP) were quantified.

Results: The FEA model demonstrated that increasing the rotational radius from 10 cm to 14 cm or 17 cm led to a significant increase in shear stress and IOP across the vitreoretinal interface and within the retinal layers. Specifically, shear stress in the preretinal layer increased by 70.2% (8.0 kPa vs. 4.7 kPa), in the intraretinal layer by 20.0% (5.4 kPa vs. 4.5 kPa), and in the subretinal layer by 6.1% (3.5 kPa vs. 3.3 kPa). Simultaneously, IOP in the central region increased by 157.5% (39.4 mmHg vs. 15.3 mmHg) and in the posterior region by 162.3% (41.7 mmHg vs. 15.9 mmHg) when the rotational radius was increased to 17 cm from 10 cm. Increasing the rotational radius to 17 cm led to more pronounced changes in peak IOPs, with the central region showing a change of 39.4 mmHg and the posterior region a change of 41.7 mmHg. These results indicate a direct correlation between the rotational radius and the magnitude of IOP changes in the vitreous.

Conclusions: These findings highlight the critical impact of rotational radius on the biomechanical forces exerted within the eye during asymmetrical shaking events, leading to variations in shear stress and IOP that could contribute to unilateral retinal hemorrhage in SBS. These insights reveal the complexity of diagnosing SBS and emphasize the need for careful consideration of the biomechanical evidence in patients presenting with asymmetrical or unilateral retinal hemorrhage.

KEYWORDS

finite element analyses, shaken baby syndrome, child abuse, ora serrata, retina, scleras, vitreous humor, retinal hemorrhages, asymmetrical retinal hemorrhages

Correspondence: Linxia Gu, Department of Biomedical Engineering and Science, Florida Institute of Technology, Melbourne, FL, USA. Email: gul@fit.edu ORCID iD: https://orcid.org/0000-0003-2637-0299, and Donny W. Suh. Gavin Herbert Eye Institute, Department of Ophthalmology, University of California, Irvine, CA, USA. Email: donnys@hs.uci.edu. ORCID iD: https://orcid.org/0000-0003-0348-2060

How to cite this article: Choi HEH, Colmenarez JA, Hong JD, Shahraki K, Gu L, Suh DW. Finite element analysis of asymmetrical retinal hemorrhages in shaken baby syndrome. Med Hypothesis Discov Innov Ophthalmol. 2025 Spring; 14(1): 231-238. https://doi.org/10.51329/mehdiophthal1514

Received: 21 December 2024; Accepted: 18 March 2025



Copyright © Author(s). This is an open-access article distributed under the terms of the Creative Commons Attribution-NonCommercial 4.0 International License (https://creativecommons.org/licenses/by-nc/4.0/) which permits copy and redistribute the material just in noncommercial usages, provided the original work is properly cited.

INTRODUCTION

Retinal hemorrhage in infants has long been a crucial diagnostic indicator of suspected child abuse, particularly shaken baby syndrome (SBS). Originally described by Caffey in the 1970s, SBS is predominantly associated with bilateral retinal hemorrhages [1-4]. This bilateral manifestation has been the cornerstone of clinical evaluation and legal deliberations concerning child abuse. However, recent clinical observations indicate that the presence of unilateral retinal hemorrhages does not necessarily exclude SBS [5, 6]. Understanding these occurrences is vital because misinterpretation may lead to diagnostic and judicial misjudgments.

The prevalence of unilateral retinal hemorrhage in SBS cases, although less common than in bilateral presentations, is not negligible. Previous studies have documented that 14%–21% of SBS cases present with unilateral retinal hemorrhages [7-9]. This poses a challenge to the accurate diagnosis of SBS, complicating both clinical and legal assessments. This complexity is further heightened by the myriad causes of retinal hemorrhages, ranging from benign conditions to more severe traumatic events [10]. This ambiguity necessitates a deeper exploration of the biomechanical underpinnings of such events.

Retinal hemorrhages resulting from abusive head trauma increase the odds of various long-term visual and ocular complications, including amblyopia, strabismus, and cortical visual impairment [11]. Biomechanical computational analyses can reveal the mechanistic details of how abusive head trauma can lead to not only unilateral retinal hemorrhage but also ocular structural compromise that predisposes the eye to downstream complications [1, 2].

By employing a finite-element model of the eye [2], this study meticulously replicated the conditions of asymmetrical shaking forces, a scenario hypothesized to underlie cases of unilateral retinal hemorrhage in SBS [2]. The simulation focused on delineating the changes in pressure and tension within the retinal vasculature, thereby offering insights into the potential mechanisms underlying such clinical presentations. The etiology of unilateral retinal hemorrhage in SBS remains largely speculative because of the absence of a detailed biomechanical analysis. This study aimed to bridge this gap using a computational approach.

METHODS

Computational Simulation of Unilateral Shaking

The unilateral shaking scenario [2] was reproduced through a finite element analysis (FEA) using Abaqus/Explicit 2023 (Dassault Systemes Simulia Corp., Providence, RI, USA), as detailed in the Abaqus licensing documentation [12]. A simplified eye model was generated to evaluate the shear forces acting on the vitreoretinal interface during shaking. The model included important ocular structures such as the sclera, vitreous, and retina (Figure 1A). The sclera and retina were modeled as spherical shells with outer diameters of 26 mm and 24.5 mm, and thicknesses of 0.8 mm and 0.25 mm, respectively (Figure 1A-C) [12].

To assess the stress-strain response at the preretinal, intraretinal, and subretinal locations (Figure 1C), we divided the retinal mesh into three equally spaced layers with an element height of 0.083 mm. The remaining space within the retina was filled with the vitreous humor and attached to it via the main retinal vessels extracted from a standard fundus image [13], as shown in Figure 1B. The sclera and the retina were connected using tie constraints at their interfaces to prevent any relative motion between them. A surface-based tie constraint was applied at the interface between the vitreous and retinal surfaces, including elements corresponding to the retinal arteries. This constraint ensures that all degrees of freedom at the interface move together, preventing any independent motion and thereby accurately mimicking the anatomical attachment between the retinal vessels and the vitreous. This constraint also facilitates the creation of two independently generated meshes with varying levels of refinement, without the need to share nodes at the interface.

Regarding the simulation's nature, both the simulation and the shaking scenario are dynamic, as indicated by the use of the Abaqus/Explicit solver package [12], which inherently supports dynamic simulations. In contrast, the vitreous was attached to the posterior retina via the main retinal vessels (Figure 1B). A general contact formulation was considered for vitreoretinal regions without adhesions. Weaker adhesive forces in the vitreoretinal regions outside the vessel locations justify the omission of this behavior. A total of 17 856 linear hexahedral elements with reduced integration (C3D8R) were adopted in the eye model to ensure accurate results. The constitutive models of these tissues, along with their respective material properties, were adopted from our earlier studies on mechanical tests of sheep eyes [14]. Weaker adhesive forces in the vitreoretinal regions outside the vessel locations justify the omission of this behavior. An in-depth description of the experimental procedure can be found in Song et al. study [14]. The material properties are listed in Table 1.

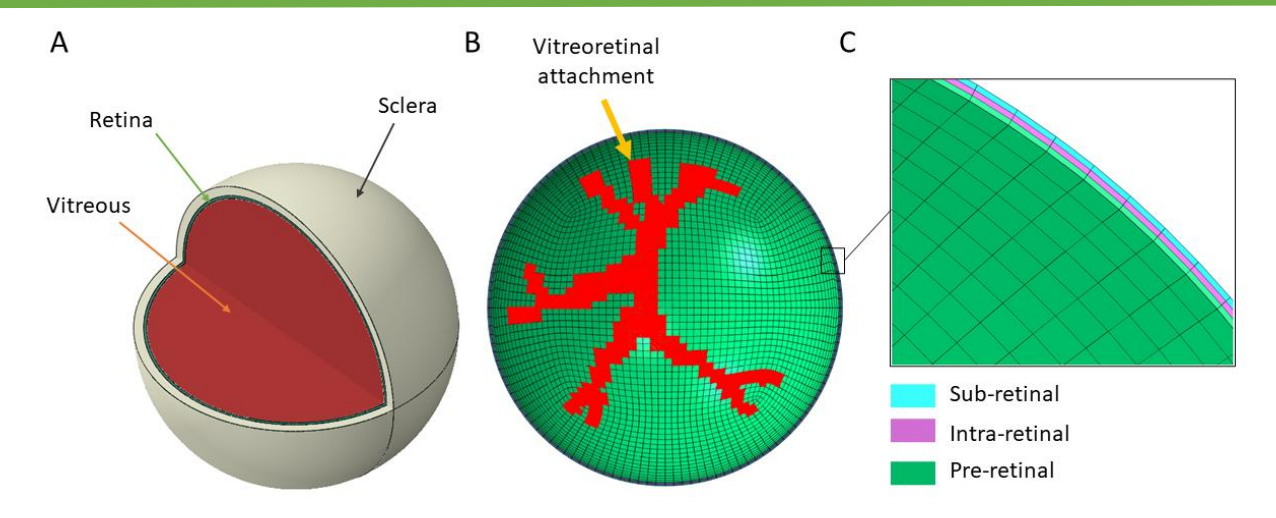


Figure 1. Simplified finite element analysis (FEA) model. (A) Ocular components of the model, including vitreous, retina, and sclera. (B) Retinal mesh and node attachments to the vitreous humor. (C) Retinal layers including the preretinal, intraretinal, and subretinal layers.

Table 1. Summary of material properties for the ocular tissues

Ocular tissue	Constitutive model	Material parameters
Sclera	Isotropic hyperelastic: 2 nd order polynomial	Uniaxial test data [14]
Retina	Isotropic linear elastic	E = 20 kPa, v = 0.49
Vitreous humor	Isotropic linear elastic with Prony-type viscoelasticity	$E = 0.03 \ Pa, \ v = 0.5, \ g_i = 0.97, \ k_i = 0, \ \tau_i = 0.07$

E, Young's modulus; v, Poisson's ratio; g_i , k_i , and τ_i . Coefficients defining the Prony series for the viscoelastic responses. Note: The vitreous humor was modeled as a viscoelastic material, incorporating both elastic and time-dependent viscous behavior. To capture this response, the Prony series was employed to represent the material's viscoelastic properties. However, because the viscoelastic formulation inherently depends on an underlying elastic response, an isotropic linear elastic constitutive model was also defined. This elastic component is essential for simulating the long-term or quasistatic behavior of the vitreous and is required by the solver to enable the time-dependent viscoelastic analysis.

The proposed mechanism responsible for the asymmetric loadings in the eye lies in the generated rotational movement of the child's head by either stronger shaking of the preparer's hand preference or secondary lateral rotations of the neck [15]. In this analysis, the rotational movement of the eye structure (including the sclera, retina, and vitreous) was simulated by applying acceleration boundary conditions consistent with pendulum-like motion, as determined by the distance between the eyes and the center of head rotation. No additional static constraints are imposed. The shear stresses observed in the retina emerged solely because of dynamic acceleration, confirming that these boundary conditions were sufficient to capture the stress distribution under the modeled shaking scenario. The acceleration affecting the eyes owing to these rotational movements is closely tied to the distance between the eyes and the center of rotation of the head. Therefore, we hypothesized that eyes situated farther from this pivotal point would encounter significantly greater forces than those positioned closer to the pivot point. To substantiate this hypothesis, we conducted three shaking simulations in which the eye was subjected to pendulum-like movements with rotation radii of 10, 14, and 17 cm, to assess the increase in stress across the vitreoretinal interface (Figure 2). A radius of 10 cm approximates the distance between the proximal eye and the perpetrator's hand, whereas a radius of 14 or 17 cm reflects the distance between the distal eye and the perpetrator's hand, accounting for variations in infant size (Figure 2). The variation in angular position is given by a sinusoidal motion:

$$\theta(t) = \theta_{max} \sin(2\pi f t) (1)$$

where θ_{max} is the maximum head rotation, f is the shaking frequency, and t is the time. Both shaking scenarios were designed to reproduce full rotation of the neck, with a maximum value of 90°. We assumed that the shaking motion followed a pendulum-like trajectory [16], as represented by the equation This reproduces the oscillatory behavior of the shaking motion, which is well known from experimental measurements.

A shaking frequency of 1 Hz was selected to mimic moderate agitation of the head. Variations in the maximum shear stress imparted to the retina and increases in intraocular pressure (IOP) within the vitreous were continuously monitored throughout a complete shaking cycle.

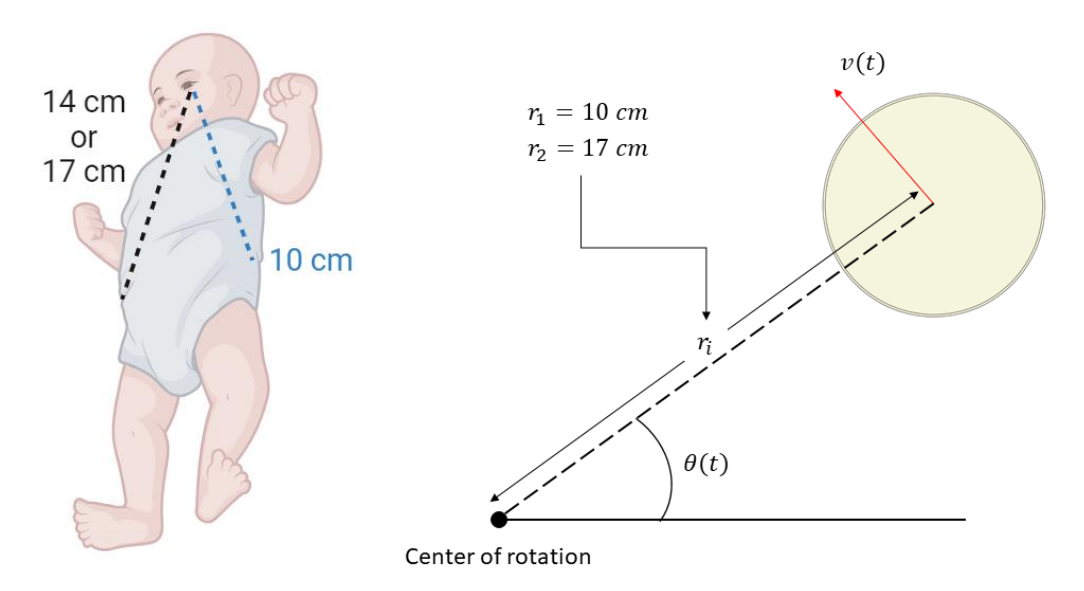


Figure 2. Rotational shaking of the eye is implemented in the finite element analysis (FEA) model. $\theta(t)$ represents the change in angular position, r_i the rotation radius, and v(t) the velocity vector. Note: The rotational radii of 14 cm, 17 cm, and 10 cm represent the estimated distances from the rotational hinge point at the hip to the corresponding positions of the eyes in the modeled scenarios. These values were used to define the arc lengths through which the head and eyes would travel during simulated whole-body rotational motion.

RESULTS

Distribution of Stress in the Vitreoretinal Interface, Retina, and Retinal Vessels under Different Rotational Radii

Head rotation involving both the dominant and non-dominant hands leads to varying radii of rotation exerted on the eye. We hypothesized that eyes positioned further from the pivot point would encounter greater forces and stress than those positioned closer. To evaluate this, three different rotation radii (10, 14, and 17 cm) were used to assess the stress across the vitreoretinal interface using FEA. Higher shear stresses related to tangential forces acting on the retina were generated with a rotational radius of 14 or 17 cm than with 10 cm (Figure 3). The distribution of von Mises stress is directly related to the shear action exerted by the vitreous on the retina. Although the shear-stress components can be reported individually, their values depend on the orientation of the coordinate system, which complicates direct comparisons across different simulation setups. Therefore, the von Mises stress was used as a scalar measure to evaluate the mechanical response because it is invariant to coordinate transformations and effectively captures the shear-dominated state of stress. This makes it suitable for assessing shear effects, particularly under conditions in which the stress tensor may approach a pure shear state. Angular acceleration generated the maximal stress along the retinal vasculature (Figure 3).

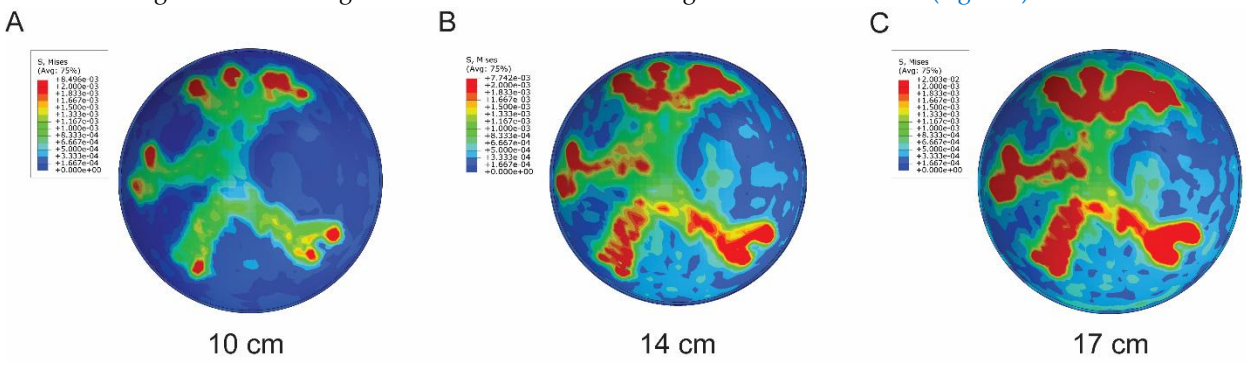


Figure 3. The distribution of von Mises stress in the vitreoretinal interface, retina, and retinal vessels under different rotation radii. (A) Stress distribution with a rotation radius of 10 cm. (B) Stress distribution with a rotation radius of 17 cm.

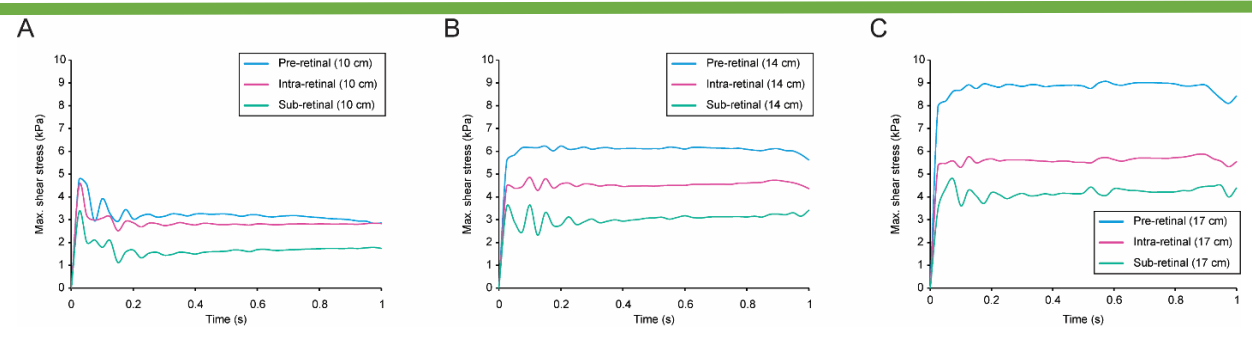


Figure 4. Maximum shear stress changes in the retinal layers at different time points under different rotation radii. (A) Maximum sheer stress distribution with a rotation radius of 10 cm. (B) Maximum sheer stress distribution with a rotation radius of 17 cm.

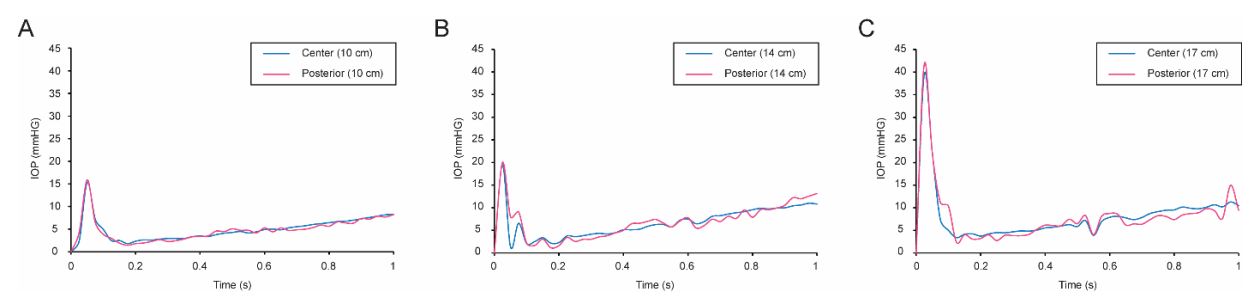


Figure 5. Intraocular pressure (IOP) changes at the central and posterior vitreous. (A) IOP changes with a rotational radius of 10 cm. (B) IOP changes with a rotational radius of 14 cm. (C) IOP changes with a rotation radius of 17 cm.

Changes in Maximum Shear Stress Across Retinal Layers at Different Rotational Radii

The FEA model was used to assess the changes in the maximum shear stress across the retinal layers, revealing distinct stress profiles under varying rotational radii (Figure 4). At a rotational radius of 10 cm, the maximum shear stresses observed in the preretinal, intraretinal, and subretinal layers were 4.7, 4.5, and 3.3 kPa, respectively. When the rotational radius increased to 14 cm, the maximum shear stresses in these layers were 5.6, 4.5, and 3.6 kPa, respectively. An increase in the rotational radius to 17 cm resulted in a substantial increase in shear stress within these layers, with values of 8.0, 5.4, and 3.5 kPa, respectively. The most pronounced difference was observed in the preretinal layer, exhibiting a 70.2% increase (8.0 kPa vs. 4.7 kPa), followed by the intraretinal layer with a 20.0% increase (5.4 kPa vs. 4.5 kPa), and the subretinal layer with a 6.1% increase (3.5 kPa vs. 3.3 kPa) when the rotation radius increased from 10 to 17 cm. In addition, the FEA model was used to measure the average retinal stress over time. An increase in the rotational radius from 10 to 14 cm resulted in increases of 88%, 58%, and 79% in the average retinal stress in the preretinal, intraretinal, and subretinal layers, respectively. Similarly, an increase in the rotational radius of 17 cm led to increases of 173%, 95%, and 146%, respectively, in these layers. These findings demonstrate the significant impact of longer rotational radii on shear stress distribution across the vitreoretinal interface and within different retinal layers.

Intraocular Pressure Variations in Response to Different Rotational Radii

The FEA model was utilized to investigate the changes in IOP associated with different rotational radii, demonstrating the impact on IOP variations within the vitreous (Figure 5). At a rotational radius of 10 cm, the maximum change in IOP in the central region was 15.3 mmHg, and the posterior regions closer to the optic nerve showed a change of 15.9 mmHg. At a rotational radius of 14 cm, the maximum changes in IOP were 19.5 and 19.9 mmHg. Increasing the rotational radius to 17 cm led to more pronounced changes in peak IOPs, with the central region showing a change of 39.4 mmHg and the posterior region a change of 41.7 mmHg. The increase to a 17 cm rotational radius resulted in a 157.5% increase (39.4 mmHg vs. 15.3 mmHg) in the central region and a 162.3% increase (41.7 mmHg vs. 15.9 mmHg) in the posterior region compared to the 10 cm rotational radius. These results indicate a direct correlation between the rotational radius and the magnitude of IOP changes in the vitreous.

DISCUSSION

This study highlights the ocular structures that require long-term monitoring for proper development and function from childhood to adulthood. This study is pivotal in advancing our understanding of SBS, particularly in patients presenting with atypical unilateral retinal hemorrhage. The results of this study have the potential to inform and refine diagnostic

criteria, assist in the accurate interpretation of clinical findings, and contribute to more informed judicial proceedings in suspected cases of child abuse. By elucidating the biomechanical aspects of unilateral retinal hemorrhage, this study adds a critical dimension to the existing knowledge of SBS, thereby enhancing both clinical and forensic practice in this domain.

Child abuse is highly likely to be involved in cases of retinal hemorrhages [17, 18]. Although most retinal hemorrhages in SBS occur bilaterally, there have been multiple cases of unilateral hemorrhage with a confirmed history of abusive trauma by shaking [2, 15, 17]. The findings of this study provide significant insights into the biomechanical factors contributing to unilateral retinal hemorrhage in SBS.

Investigations into these biomechanics using FEA visually depict high-risk sites for ocular structural injury. The neurovascular compromise demonstrated in our study shows a pattern of injury that can render the affected eye more susceptible to long-term visual or ocular complications such as amblyopia, strabismus, or cortical visual impairment [11]. Our study highlights the potential need to monitor the affected eye for proper ocular development and retinal function using a variety of testing modalities, including microperimetry, Humphrey visual field test, refraction tests, and cover test [19-21].

Our investigation using the FEA model provides a comprehensive understanding of stress distribution and IOP variations within the vitreous, vitreoretinal interface, retinal layers, and retinal vessels under different rotational radii. These biomechanical analyses are crucial for elucidating the etiological underpinnings of unilateral retinal hemorrhage in patients with SBS. Although the nature of abusive shaking is not necessarily documented in cases of SBS-associated unilateral retinal hemorrhage [2], our results demonstrate the contribution of rotational forces in the differential stresses sustained by the retinal vasculature of each eye. The application of three distinct rotational radii—10, 14, and 17 cm—in our simulations highlighted the critical role of the rotational radius in the generation of shear stresses and variations in the IOP. Notably, the increase in rotational radius to 17 cm resulted in significantly higher shear stresses across the vitreoretinal interface and within the various retinal layers, as well as marked increases in IOP. These results support the hypothesis that the eye positioned further from the pivot point, thereby simulating the effect of shaking with both hands, encounters greater forces, leading to higher stress and IOP changes in the central and posterior vitreous regions.

The pronounced increase in shear stress and IOP with longer rotational radii clearly demonstrates the heightened risk of tissue damage and hemorrhage under such conditions. This biomechanical evidence supports the assertion that unilateral or asymmetric retinal hemorrhages in SBS [22] may indeed result from asymmetrical force application, a scenario that can occur when an infant is shaken at varying intensities or angles of force exerted by the dominant and non-dominant hands. Additionally, the complexity of the injury could be exacerbated if shaking involves direct physical contact of the infant's head with a hard surface. The association of unilateral retinal hemorrhage with SBS is further supported by the presence of ipsilateral cerebral hemorrhage or infarct in multiple clinical cases of reported abusive trauma [5, 15]. Our results on differential shear stresses dependent on the rotational radius help elucidate the mechanism for ipsilateral presentation of both cerebral and retinal hemorrhages from shaking [2, 22].

Furthermore, the significant differences observed in the shear stress profiles within the retinal layers between the two rotational radii highlighted the importance of the mechanical aspects of shaking in the diagnosis and understanding of SBS. The data from this study contribute to a more nuanced understanding of the biomechanical mechanisms underlying unilateral retinal hemorrhage, offering a pathway toward refining the diagnostic criteria for SBS. This is particularly relevant in cases in which retinal hemorrhage deviates from the traditionally expected bilateral pattern, thereby challenging the conventional diagnostic framework [23]. These results are consistent with the clinical observations of SBS-related retinal hemorrhages with multilayer involvement extending from the preretinal to the subretinal layer [18, 22].

The elevation in shear stress and IOP directly contributes to the pathophysiology of retinal hemorrhage, as demonstrated by the simulation results. The FEA model revealed that the angular acceleration generated maximal shear stress along the retinal vasculature [24]. Shear stress can disrupt the integrity of the retinal vasculature, particularly in delicate capillary networks, leading to vascular compromise and subsequent superficial and deep intraretinal hemorrhages. Similarly, acutely elevated IOP can cause a direct mechanical insult to retinal vessels, exacerbating vascular fragility and promoting leakage or rupture. Paradoxically, an increased IOP may exert a tamponading effect, preventing further bleeding [24]. The FEA model demonstrated that the eye farther from the pivot point was subjected to a higher acceleration, thereby generating increased shear stress at the vitreoretinal interface. This effect is attributed to the tangential forces acting on the retina, with the shear motion of the vitreous against the retina playing a pivotal role in stress development. Notably, the analysis revealed elevated stresses in the anterior retinal layer compared with those in

the posterior layer, highlighting the critical influence of vitreous shear in facilitating retinal hemorrhage. Additionally, elevated stress at the vitreoretinal interface can facilitate vitreous traction, which in turn can lead to retinal detachment and hemorrhage. These mechanical stresses, when applied asymmetrically, as our model suggests, can result in unilateral retinal hemorrhages observed in some SBS cases, providing a biomechanical explanation for these clinical findings [22].

Although this study provided valuable insights into the biomechanical aspects of unilateral retinal hemorrhage in SBS through computational simulations, it is important to acknowledge its limitations. The simulations were performed based on specific rotational radii, which, although offering important insights, may not encompass the full range of forces or scenarios encountered in real-life SBS cases. Additionally, certain complexities of the human eye and the dynamic nature of shaking forces may not be fully captured by the model. Owing to the complexity of the computational models, each simulation required up to 48 h for completion, indicating a significant investment in time and computational resources. The potential effects of variations in material properties and shaking conditions on retinal stress were not assessed because of the computational expense required to gather adequate data. Further controlled experiments with dummy dolls should be performed to capture the acceleration variance between the eyes and validate these findings. Additionally, a retrospective analysis of clinical data is required to validate these results. Notwithstanding these limitations, the findings from this study contribute significantly to our understanding of the biomechanical forces at play in the etiology of unilateral retinal hemorrhages and underscore the need for further experimental and clinical research to validate and expand upon these computational results.

CONCLUSIONS

This study underscores the need for a multidisciplinary approach to investigate SBS, integrating biomechanical analyses with clinical observations to enhance diagnostic accuracy. The insights gained from our computational simulation emphasize the variability in injury mechanisms and underscore the complexity of accurately diagnosing SBS based solely on the bilateral, asymmetrical, or unilateral presentation of retinal hemorrhages. Our findings advocate the inclusion of biomechanical evidence in forensic and clinical evaluations of suspected child abuse cases, potentially leading to more informed judicial proceedings and improved outcomes for affected individuals. Our mechanistic study depicts the pattern of neurovascular injury and highlights the need for continued monitoring of the affected eye to ensure proper ocular development and retinal function. This is crucial for preventing complications that can result in permanent vision loss. By addressing the biomechanical aspects of unilateral retinal hemorrhage, this study adds a critical dimension to the existing knowledge of SBS, contributing to the enhancement of both clinical and forensic practice in this domain. Further research is warranted to explore the full spectrum of biomechanical factors involved in SBS to facilitate the development of comprehensive diagnostic and therapeutic strategies.

ETHICAL DECLARATIONS

Ethical approval: No human subjects were included in this study. All the procedures were performed in accordance with the Declaration of Helsinki and did not involve human or animal subjects. The UCI Institutional Review Board Committee determined that the study did not qualify as human subject research and waived the requirement for informed consent. No animal subjects were included in this study.

Conflict of interest: None.

FUNDING

None.

ACKNOWLEDGMENTS

None.

REFERENCES

- Colmenarez JA, Lam M, Dong P, Hoskin AK, Agrawal RV, Shahraki K, Suh DW, Gu L. Comparative biomechanical study of blunt ocular traumas and shaken baby syndrome. Investigative Ophthalmology & Visual Science. 2024 Jun 17;65(7):2877-. Link
- Shahraki K, Suh DW. An Update to Biomechanical and Biochemical Principles of Retinal Injury in Child Abuse. Children (Basel). 2024 May 12;11(5):586. doi: 10.3390/children11050586. PMID: 38790581; PMCID: PMC11119297.
- Gabaeff SC. Challenging the Pathophysiologic Connection between Subdural Hematoma, Retinal Hemorrhage and Shaken Baby Syndrome. West J Emerg Med. 2011 May;12(2):144-58. PMID: 21691518; PMCID: PMC309959.

- Levin AV. Ophthalmology of shaken baby syndrome. Neurosurg Clin N Am. 2002 Apr;13(2):201-11, vi. doi: 10.1016/s1042-3680(02)00004-9. PMID: 12391704.
- 5. Arlotti SA, Forbes BJ, Dias MS, Bonsall DJ. Unilateral retinal hemorrhages in shaken baby syndrome. J AAPOS. 2007 Apr;11(2):175-8. doi: 10.1016/j.jaapos.2006.09.023. Epub 2007 Feb 15. PMID: 17306998.
- Sornalingam K, Borman AD, Ashworth J. Nonaccidental injury presenting as unilateral retinal detachment in two infants. J AAPOS. 2018 Jun;22(3):231-233. doi: 10.1016/j.jaapos.2017.10.018. Epub 2018 Feb 2. PMID: 29410140.
- 7. Wilkinson WS, Han DP, Rappley MD, Owings CL. Retinal hemorrhage predicts neurologic injury in the shaken baby syndrome. Arch Ophthalmol. 1989 Oct;107(10):1472-4. doi: 10.1001/archopht.1989.01070020546037. PMID: 2803095.
- 8. Morad Y, Kim YM, Armstrong DC, Huyer D, Mian M, Levin AV. Correlation between retinal abnormalities and intracranial abnormalities in the shaken baby syndrome. Am J Ophthalmol. 2002 Sep;134(3):354-9. doi: 10.1016/s0002-9394(02)01628-8. PMID: 12208246.
- 9. Kivlin JD, Simons KB, Lazoritz S, Ruttum MS. Shaken baby syndrome. Ophthalmology. 2000 Jul;107(7):1246-54. doi: 10.1016/s0161-6420(00)00161-5. PMID: 10889093.
- Khosravi P, Huck NA, Shahraki K, Hunter SC, Danza CN, Kim SY, Forbes BJ, Dai S, Levin AV, Binenbaum G, Chang PD, Suh DW. Deep Learning Approach for Differentiating Etiologies of Pediatric Retinal Hemorrhages: A Multicenter Study. Int J Mol Sci. 2023 Oct 12;24(20):15105. doi: 10.3390/ijms242015105. PMID: 37894785; PMCID: PMC10606803.
- 11. Weldy E, Shimoda A, Patnaik J, Jung J, Singh J. Long-term visual outcomes following abusive head trauma with retinal hemorrhage. J AAPOS. 2019 Dec;23(6):329.e1-329.e4. doi: 10.1016/j.jaapos.2019.08.276. Epub 2019 Oct 23. PMID: 31655114.
- Dassault Systèmes. Licensed Program Specifications (LPS) for Abaqus 2023. Providence (RI): Dassault Systèmes Simulia Corp.;
 2022. Available at: https://docs.software.vt.edu/abaqusv2024/English/SIMACAEGSARefMap/simagsa-c-intdoc.htm?utm_source=chatgpt.com (Accessed: February 20, 2025).
- 13. Suh DW, Song HH, Mozafari H, Thoreson WB. Determining the Tractional Forces on Vitreoretinal Interface Using a Computer Simulation Model in Abusive Head Trauma. Am J Ophthalmol. 2021 Mar;223:396-404. doi: 10.1016/j.ajo.2020.06.020. Epub 2020 Jul 12. PMID: 32663454.
- 14. Song HH, Thoreson WB, Dong P, Shokrollahi Y, Gu L, Suh DW. Exploring the Vitreoretinal Interface: A Key Instigator of Unique Retinal Hemorrhage Patterns in Pediatric Head Trauma. Korean J Ophthalmol. 2022 Jun;36(3):253-263. doi: 10.3341/kjo.2021.0133. Epub 2022 May 6. PMID: 35527527; PMCID: PMC9194735.
- 15. Drack AV, Petronio J, Capone A. Unilateral retinal hemorrhages in documented cases of child abuse. Am J Ophthalmol. 1999 Sep;128(3):340-4. doi: 10.1016/s0002-9394(99)00147-6. PMID: 10511029.
- Yamazaki J, Yoshida M, Mizunuma H. Experimental analyses of the retinal and subretinal haemorrhages accompanied by shaken baby syndrome/abusive head trauma using a dummy doll. Injury. 2014 Aug;45(8):1196-206. doi: 10.1016/j.injury.2014.04.014. Epub 2014 Apr 16. PMID: 24810668.
- Binenbaum G, Mirza-George N, Christian CW, Forbes BJ. Odds of abuse associated with retinal hemorrhages in children suspected of child abuse. J AAPOS. 2009 Jun;13(3):268-72. doi: 10.1016/j.jaapos.2009.03.005. PMID: 19541267; PMCID: PMC2712730.
- 18. Moskwa R, Todeschi J, Wiedemann-Fode A, Stella I, Joud A, Klein O. Ophthalmological lesions in shaken baby syndrome: A retrospective analysis of 133 consecutive cases (1992-2018). Neurochirurgie. 2022 Jul;68(4):367-372. doi: 10.1016/j.neuchi.2022.01.007. Epub 2022 Feb 9. PMID: 35150727.
- 19. Zhou J, Liu W, Li X, Li Q, Hao J, Wang XL. [Macular retinal function detected by MP-1 microperimetry in normal subjects of middle and old age]. Zhonghua Yan Ke Za Zhi. 2011 Jan;47(1):35-8. Chinese. PMID: 21418925.
- 20. Thakur U, Thattaruthody F, Gupta G, Singh AK, Chaurasia S, Pandav SS, Kaushik S. Visual field indices in children and adults with comparable retinal nerve fiber layer thickness. J AAPOS. 2023 Aug;27(4):203.e1-203.e7. doi: 10.1016/j.jaapos.2023.06.002. Epub 2023 Jul 11. PMID: 37442537.
- 21. Committee on Practice and Ambulatory Medicine, Section on Ophthalmology. American Association of Certified Orthoptists; American Association for Pediatric Ophthalmology and Strabismus; American Academy of Ophthalmology. Eye examination in infants, children, and young adults by pediatricians. Pediatrics. 2003 Apr;111(4 Pt 1):902-7. PMID: 12671132.
- 22. Healey K, Schrading W. A case of shaken baby syndrome with unilateral retinal hemorrhage with no associated intracranial hemorrhage. Am J Emerg Med. 2006 Sep;24(5):616-7. doi: 10.1016/j.ajem.2005.11.016. PMID: 16938603.
- 23. Khosravi P, Huck NA, Shahraki K, Ghafari E, Azimi R, Kim SY, Crouch E, Xie X, Suh DW. External Validation of Deep Learning Models for Classifying Etiology of Retinal Hemorrhage Using Diverse Fundus Photography Datasets. Bioengineering (Basel). 2024 Dec 29;12(1):20. doi: 10.3390/bioengineering12010020. PMID: 39851294; PMCID: PMC11760437.
- 24. Hong JD, Colmenarez JA, Choi EH, Suh A, Suh A, Lam M, Hoskin A, Minckler DS, Lin KY, Shahraki K, Agrawal R, Dong P, Gu L, Suh DW. Finite Element Analysis of Mechanical Ocular Sequelae from Badminton Shuttlecock Projectile Impact. Ophthalmol Sci. 2024 Sep 19;5(1):100625. doi: 10.1016/j.xops.2024.100625. PMID: 39624794; PMCID: PMC11609241.